Eur. Phys. J. D (2018) 72: 228
https://doi.org/10.1140/epjd/e2018-90096-8

THE EUROPEAN PHYSICAL JOURNAL D

Regular Article

Excitation of strongly interacting moving Rydberg atoms by photon recoil momentum

Razmik G. Unanyan[a]

Fachbereich Physik, Technische Universität Kaiserslautern, 67663 Kaiserslautern, Germany

Received 5 March 2018 / Received in final form 10 October 2018
Published online 21 December 2018

Abstract. Based on the fact that an ensemble of moving Rydberg atoms in two counterpropagating laser beams in the limit of complete dipole blocking is isomorphic to a Jaynes–Cummings model, a scheme for robust and efficient excitation of atomic Rydberg states is proposed. It is shown that the Doppler frequency shifts play an important role in atomic population transfer processes. The suggested method can be employed to detect the symmetric entangled states and paves the way to preparing entangled states with a single excited atom in a Rydberg state. It is shown that this process is robust with respect to parameter fluctuations, such as the laser pulse area, the relative spatial offset (the delay) of the laser beams and the number of atoms.

1 Introduction

Strongly interacting ultracold Rydberg atoms are promising candidates for creating many-body entangled states [1–3]. Such states are a resource for quantum-information processing protocols [4]. In mesoscopic atomic systems the entangled states, as a rule, become increasingly susceptible to fluctuations of internal and external parameters especially to the number of atoms N. And therefore an important practical challenge is the design of robust methods for generating entangled many-body states in strongly interacting Rydberg atoms. Several robust approaches have been proposed based on the stimulated adiabatic passage methods [5–7] to transfer atoms from their ground (product) state into Rydberg excited (entangled) states (see [8,9]). More details about methods relying on adiabatic processes in ultracold Rydberg gases can be found e.g. in the review article by Saffman et al. [3]. Both schemes [8] and [9] (see also [10] and [11]) are based on the fact that ensembles of Rydberg atoms in resonant laser fields in the limit of complete dipole blocking [2] are isomorphic to a Jaynes–Cummings model [12,13]. A robust method to generate entangled states has been proposed in [8] for an ensemble of three-level atoms in Lambda configuration [14] where the Rydberg state $|r\rangle$ couple nearly resonantly by laser fields to two stable states $|a\rangle$ and $|b\rangle$. The suggested method, unlike the scheme in [9], works equally well for even and odd number of atoms. Exact knowledge of the number of particles is not required, making the method robust against atom number fluctuations. In particular, it was shown in [8] that the symmetric entangled state

$$|bb...br\rangle_S = \frac{1}{\sqrt{N}}\left(|rb\cdots b\rangle + |br\cdots b\rangle \cdots + |b\cdots br\rangle\right) \quad (1)$$

can be created from the product ground state $|aa\cdots a\rangle$. Here, the subscript "S" indicates symmetrization over all atoms and makes the state totally symmetric. The studies in [8], however, indicate that the required laser fields (Rabi frequencies) scale nearly as $\sqrt{N}$, hence this method can only be applied to sufficiently small atomic systems. From the quantum information perspective the state (1) up to local unitary transformations is, however, equivalent to the state

$$|aa...ar\rangle_S = \frac{1}{\sqrt{N}}\left(|ra\cdots a\rangle + |ar\cdots a\rangle \ldots + |a\cdots ar\rangle\right). \quad (2)$$

In the present paper, we consider the possibility to create this less costly entangled state compare to (1). Since for very large Rabi frequencies (in order of $\sqrt{N}$) the final state of the system is (1), it is clear, that a robust transition from the product state $|aa\cdots a\rangle$ to the state (2) is possible only within certain range of Rabi frequencies. The present paper addresses two questions: first, how to detect and distinguish experimentally these symmetric states, and second, is it possible to excite the entangled state (2) in a robust and scalable way.

In order to answer the first question, we consider the strongly interacting moving Rydberg atoms crossing two counterpropagating laser beams. In the center-of-mass system, the atoms interact nearly resonantly (due to Doppler shifts) with two laser beams. The proposed model

[a] e-mail: unanyan@physik.uni-kl.de

is a modified version of the model discussed in [8]. Because, the symmetric atomic states have different photon recoil momenta (compared to the initial product state $|aa\cdots a\rangle$), a time-of-flight analysis of atoms can be used to detect and select final symmetric entangled states by measuring shift (displacement) of the centre of mass of an atomic cloud with in situ imaging.

The second question concerning the robustness of creating the state (2) is addressed by using the fact that an ensemble of Rydberg atoms in the limit of complete dipole blocking [2] is isomorphic to a Jaynes–Cummings model. Based on this model, we show that, for fast atoms (the Doppler shift much larger than the photon recoil energy) the state (2) can be created by two laser pulses with peak amplitudes independent of the system size. Moreover, the present work shows that there exist a quite wide region of the laser pulse parameters (peak amplitudes and time delay between pulses) where varying these parameters has virtually no effect on the final state (2) of atoms and its momentum. The width of this region is strongly dependent on the Doppler shift, but not sensitive to the number of atoms.

2 Model

We consider an atomic beam, crossing with two laser beams in a volume with diameter w (see Fig. 1). In particular, we consider an atomic Λ system with three levels coupled by two counterpropagating optical fields with the same frequency ω and wave vector k whose parallel propagation axes are spatially shifted. The Rydberg state $|r\rangle$ is coupled resonantly by laser fields to two stable states $|a\rangle$ and $|b\rangle$. The initial atom velocity in the direction of the laser beams can be varied by changing the intersection angle β between atomic and laser beams (see Fig. 1). The interaction time between atoms and laser fields is assumed to be shorter than the relaxation times of the system, so that no incoherent processes (e.g., spontaneous emission back to states $|a\rangle$ and $|b\rangle$) occur. We note that this assumption is reasonable since the radiative lifetime of the Rydberg states scale with principal quantum number as n^3. For example, in alkali atoms Rydberg states with principal quantum number $50 \lesssim n \lesssim 100$ have lifetimes between $30\,\mu$s and $200\,\mu$s.

The atoms are described by spin flip operators $\sigma_{\mu\nu}^{(n)} = |\mu\rangle_n \langle\nu|$, $(\mu, \nu = a, b, r)$ and interact via the van der Waals potential $U(r) = C_6/r^6$ in the Rydberg state $|r\rangle$. Where C_6 is the van der Waals coefficient. A key quantity for the study of interacting Rydberg atoms is the blockade radius R_b, given by

$$R_b = \left(\frac{C_6}{\hbar\Omega}\right)^{1/6}, \tag{3}$$

where $\Omega = \max(\Omega_P, \Omega_S)$. Ω_P and Ω_S are the (real-valued) Rabi frequencies for the two laser fields. Using Rydberg states with principal quantum numbers $50 \lesssim n \lesssim 100$, one can realize blockade radii R_b between $1\,\mu$m and $15\,\mu$m. In the following, we assume that w is smaller than blockade radius R_b (see Fig. 1).

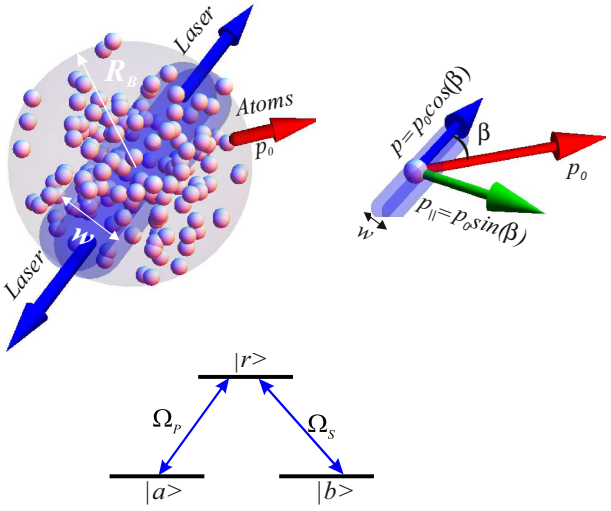

Fig. 1. Sketch of the geometry of the interaction between atoms with two counterpropagating laser fields. Three-level system with initial population in state a. The atoms have the same initial momentum p_0. The initial atom momentum in the direction of the laser beams $p = p_0 \cos\beta$ can be varied by changing the intersection angle β between atomic and laser beams. The interaction time $T = wM/(p_0 \sin\beta)$ between atoms and laser beams is much shorter than the relaxation times of the system.

In the rotating-wave approximation, the Hamiltonian of the system is given by ($\hbar = 1$)

$$H = \sum_n^N \frac{\vec{p}_n^{\,2}}{2M} + \Omega_P \sum_n^N \exp(-ikz_n)\,\sigma_{ar}^{(n)} \tag{4}$$

$$+\Omega_S \sum_n^N \exp(ikz_n)\,\sigma_{br}^{(n)} \tag{5}$$

$$+\sum_{n>m}^N \sigma_{rr}^{(n)}\sigma_{rr}^{(m)} U(|\vec{r}_n - \vec{r}_m|) + h.c. \tag{6}$$

where $\vec{p}_n$ is the momentum of nth atom. The last sum describes the interaction between atoms in the Rydberg states. Applying the gauge transformation

$$\begin{aligned} G &= \bigotimes_n^N \exp\left[ikz_n\left(\sigma_{aa}^{(n)} - \sigma_{bb}^{(n)}\right)\right] \\ &= \bigotimes_n^N \exp\left[ikz_n\sigma_{aa}^{(n)}\right]\exp\left[-ikz_n\sigma_{bb}^{(n)}\right] \\ &= \bigotimes_n^N \left[\mathbb{1} - \sigma_{aa}^{(n)}\left(1 - e^{ikz_n}\right)\right]\left[\mathbb{1} - \sigma_{bb}^{(n)}\left(1 - e^{-ikz_n}\right)\right] \\ &= \bigotimes_n^N \left[\mathbb{1} - \sigma_{aa}^{(n)} - \sigma_{bb}^{(n)} + \sigma_{aa}^{(n)}e^{ikz_n} + \sigma_{bb}^{(n)}e^{-ikz_n}\right] \\ &= \bigotimes_n^N \left[\sigma_{rr}^{(n)} + \sigma_{aa}^{(n)}\exp(ikz_n) + \sigma_{bb}^{(n)}\exp(-ikz_n)\right] \end{aligned}$$

the above Hamiltonian can be transformed into a more convenient form

$$\begin{aligned} H \rightarrow & G \cdot H \cdot G^{-1} \\ & = \sum_{n}^{N} \frac{\overrightarrow{p}_n^2}{2M} + \frac{1}{M} \sum_{n}^{N} \left(\overrightarrow{k} \cdot \overrightarrow{p}^{(n)} \right) \left(\sigma_{aa}^{(n)} - \sigma_{bb}^{(n)} \right) \\ & - \frac{k^2}{2M} \sum_{n}^{N} \sigma_{rr}^{(n)} + \Omega_P \sum_{n}^{N} \sigma_{ar}^{(n)} + \Omega_S \sum_{n}^{N} \sigma_{br}^{(n)} \\ & + \sum_{n>m}^{N} U \left(|\overrightarrow{r}_n - \overrightarrow{r}_m| \right) \sigma_{rr}^{(n)} \sigma_{rr}^{(m)} + h.c. \end{aligned} \tag{7}$$

We are interested in the case where all atoms have the same initial momentum p in the direction of the laser beams Ω_P or Ω_S and the system is initially in the product state $|aa...a\rangle = |a\rangle \otimes |a\rangle \otimes ... |a\rangle$. Taking U outside the summation sign, which corresponds to assuming the interaction to be the same between any pairs of atoms, the Hamiltonian (7) takes the form

$$\begin{aligned} H = & N \frac{p^2}{2M} + \frac{kp}{M} \sum_{n}^{N} \left(\sigma_{aa}^{(n)} - \sigma_{bb}^{(n)} \right) - \frac{k^2}{2M} \sum_{n}^{N} \sigma_{rr}^{(n)} \\ & + U_0 \sum_{n>m}^{N} \sigma_{rr}^{(n)} \sigma_{rr}^{(m)} + \Omega_P \sum_{n}^{N} \sigma_{ar}^{(n)} + \Omega_S \sum_{n}^{N} \sigma_{br}^{(n)} + h.c. \end{aligned} \tag{8}$$

Typical values for U_0 are above 10 MHz when atoms are separated less than 5 μm [3,15]. We see that the energies of atomic states $|a\rangle$ and $|b\rangle$ are shifted from the two-photon resonance by the Doppler detunings kp/M. The energy of the Rydberg state $|r\rangle$ is shifted by the recoil frequency $k^2/2M$. The interaction between the paired atoms in the Rydberg state also occurs as an energy shift, which effectively translates into the one-photon detuning.

3 Two-atoms: numerical results

In this section, the physics of the phenomenon of blockade is presented in the context of the simplest system: two interacting Rydberg atoms in two laser fields. We present the results for the two atoms obtained by numerically solving the time dependent Schrödinger equation with the Hamiltonian (8). The pulses have a Gaussian shape

$$\Omega_P(t) = \alpha e^{-\left(\frac{t+\tau}{T}\right)^2}, \ \Omega_S(t) = \alpha e^{-\left(\frac{t-\tau}{T}\right)^2}, \tag{9}$$

with equal peak Rabi frequency α and durations T. The pulses are delayed with respect to each by a time interval $\tau > 0$.

Figure 2 shows the variation of the transfer efficiency i.e. the square of the overlap between the final state and the target state $\frac{1}{\sqrt{2}}(|ar\rangle + |ra\rangle)$ for varying delay τ and varying peak Rabi frequency α for $U_0 = 60E_r$ and $p = 10k$. As can be seen in Figure 2 the population transfer is efficient over large areas of the laser pulses which is reminiscent of

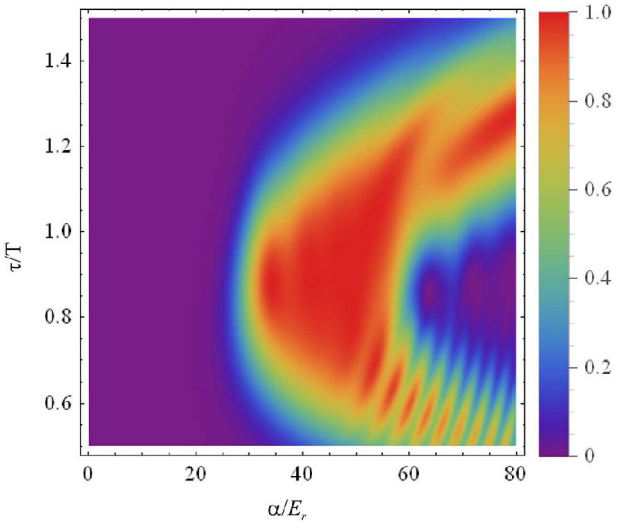

Fig. 2. Population transfer efficiency to the state $\frac{1}{\sqrt{2}}(|ar\rangle + |ra\rangle)$ for varying delay and varying peak Rabi frequency α for $p = 10k, U_0 = 60E_r$.

an adiabatic passage. It also shows a pronounced threshold peak amplitude for an efficient population transfer to the state $\frac{1}{\sqrt{2}}(|ar\rangle + |ra\rangle)$ starting at $\alpha \gtrsim 30E_r$. A large region of high transfer probability is observed for delays centered approximately at pulse widths. As will be shown below this robust feature remains the same for more than two atoms and the underlying physical mechanism is not a true adiabatic passage process. It will actually be shown that when fast atoms are localized within a region where $U_0 >> \alpha$ nearly complete population transfer from the initial state $|a \dots a\rangle$ into collective symmetric states with single Rydberg excitation takes place at a critical value of $\alpha = \alpha_c$, which does not dependent on the number of atoms. We present in the following sections explanations for these remarkable results.

4 Strongly interacting atoms

In this section, following references [8,9], the results for strongly interacting (the regime of the Rydberg blockade) Rydberg atoms are presented. The analysis of the system can be greatly simplified by employing the isomorphism between the dynamics of the Rydberg-blockaded atomic ensemble and the two mode Jaynes–Cummings model [12,13]

$$\begin{aligned} H_{\mathrm{JC}} = & \frac{kp}{M} \left(a^\dagger a - b^\dagger b \right) - \frac{k^2}{2M} \sigma^\dagger \sigma^- \\ & + \Omega_P(t) \left(a\sigma^\dagger + a^\dagger \sigma^- \right) + \Omega_S(t) \left(b\sigma^\dagger + b^\dagger \sigma^- \right), \end{aligned} \tag{10}$$

where $a^\dagger$ and $b^\dagger$ are creation operators, with bosonic commutator relations, for atoms in states $|a\rangle$ and $|b\rangle$, respectively. $\sigma^\dagger$ and σ^- describe transitions between atomic states with zero and single Rydberg excitations.

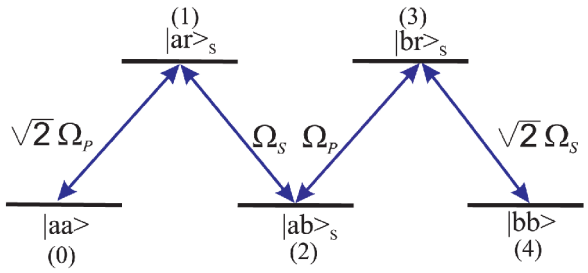

Fig. 3. Coupling scheme of collective 2-atom states in limit of dipole blockade. The symbols $(k), k = 0, 1, 2, 3, 4$ correspond to the photon recoil momenta.

In (10), the terms containing the constants of motion have been omitted. It can be easily seen that the total particle number operator

$$N = a^\dagger a + b^\dagger b + \sigma^\dagger \sigma^- \tag{11}$$

commutes with the Hamiltonian (10) so it is a conserved quantity. Using the following notations for the states: $|aa\rangle \to \frac{1}{\sqrt{2}}\left(a^\dagger\right)^2|0\rangle$, $|ab\rangle_S = \frac{1}{\sqrt{2}}(|ab\rangle + |ba\rangle) \to a^\dagger b^\dagger|0\rangle$, $|bb\rangle \to \frac{1}{\sqrt{2}}\left(b^\dagger\right)^2|0\rangle$, $|ar\rangle_S = \frac{1}{\sqrt{2}}(|ar\rangle + |ra\rangle) \to a^\dagger\sigma^+|0\rangle$ and $|br\rangle_S = \frac{1}{\sqrt{2}}(|br\rangle + |rb\rangle) \to b^\dagger\sigma^+|0\rangle$, the linkage pattern of two-atom symmetric states described by the Hamiltonian (10) can be represented pictorially as in Figure 3.

The superscript of S will be omitted hereafter for ease of notation. It is worth remarking that these atomic states can also be labeled by different photon recoil momenta, which allows the detection of these symmetric entangled states by a time-of-flight analysis of atoms. For example, for a system of two atoms one has the following correspondence $|aa\rangle \to 0$, $|ab\rangle \to 2k$, $|bb\rangle \to 4k$, $|ar\rangle \to k$, $|br\rangle \to 3k$ between external and internal degree of freedom of atoms.

In order to confirm that in the regime of the Rydberg blockade, the Hamiltonian (10) reproduces the dynamics of the primary system, we numerically integrated the Schrödinger equation with the Hamiltonian (10).

Figure 4 shows the transfer efficiency to the state $|ar\rangle$. For large α, a comparison of two plots (Figs. 4 and 2) shows essential difference, which can be attributed to the fact that as α increases the blocked condition ($U_0 >> \alpha$) is getting worse. While for relative small α they are almost identical. It is remarkable that, for a wide range of parameters the dynamics of the primary system can be well-discribed by the Jaynes–Cummings Hamiltonian (10). The isomorphism to the Jaynes–Cummings model has a number of interesting consequences. First of all, it simplifies the analysis by allowing the employment of angular momentum techniques. Second many known features of the Jaynes–Cummings dynamics can be used to produce a variety of interesting states of an atomic ensemble by the Rydberg blockade. However, despite its apparent simplicity the two-mode Jaynes–Cummings model is not an exactly solvable model.

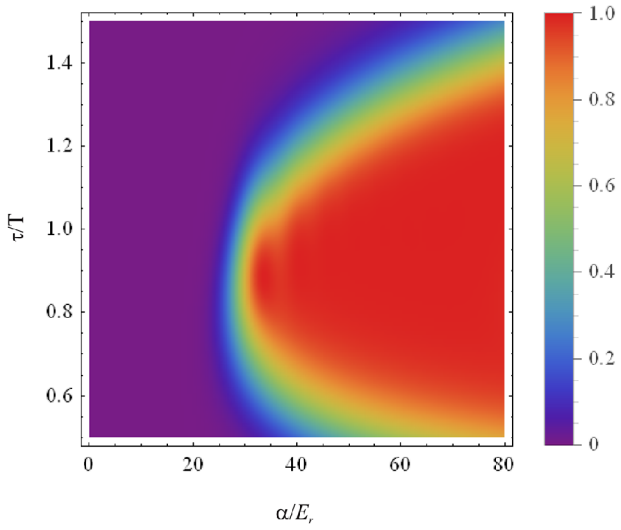

Fig. 4. Numerical integration of the Schrödinger equation with the Hamiltonian (10). The population transfer efficiency to the state $\frac{1}{\sqrt{2}}(|ar\rangle + |ra\rangle)$ for varying delay and varying peak Rabi frequency α (the other parameters are the same as in Fig. 2).

5 Two-mode Jaynes–Cummings model

5.1 Dark and bright bosons

In this section, the properties of the Hamiltonian (10) are discussed offering an explanation for the patterns shown in Figures 2 or 4 including the threshold behavior of high population-transfer efficiency. Introducing the dark and bright boson operators reference [16]

$$D = a\cos\theta - b\sin\theta, \tag{12}$$

$$B = a\sin\theta + b\cos\theta, \tag{13}$$

with $\tan\theta = \Omega_P/\Omega_S$ allows a convenient analysis of the spectrum of (10). In terms of these bosonic operators the Hamiltonian (10) reads

$$\begin{aligned} H_{\rm JC} = {} & \frac{pk}{M}\left(D^\dagger D - B^\dagger B\right)\cos 2\theta - E_r\sigma^\dagger\sigma^- \\ & + \Omega_0\left(B^\dagger\sigma^- + B\sigma^+\right) \\ & + \frac{pk}{M}\left(D^\dagger B + B^\dagger D\right)\sin 2\theta \end{aligned} \tag{14}$$

with $\Omega_0 = \sqrt{\Omega_P^2 + \Omega_S^2}$.

We note that the time dependence of populations with interactions switched on and off adiabatically ($\frac{pk}{M}T >> 1$, $\Omega_0 T >> 1$) can be discussed based on the instantaneous eigenstates of the time-varying Hamiltonian (15) (i.e. in the adiabatic basis). For fast atoms ($p >> k$) the second term in (15) is proportional to the recoil energy E_r and thus can be neglected. For ease of notation from this point onwards, the recoil frequency and momentum are used for the units of corresponding quantities.

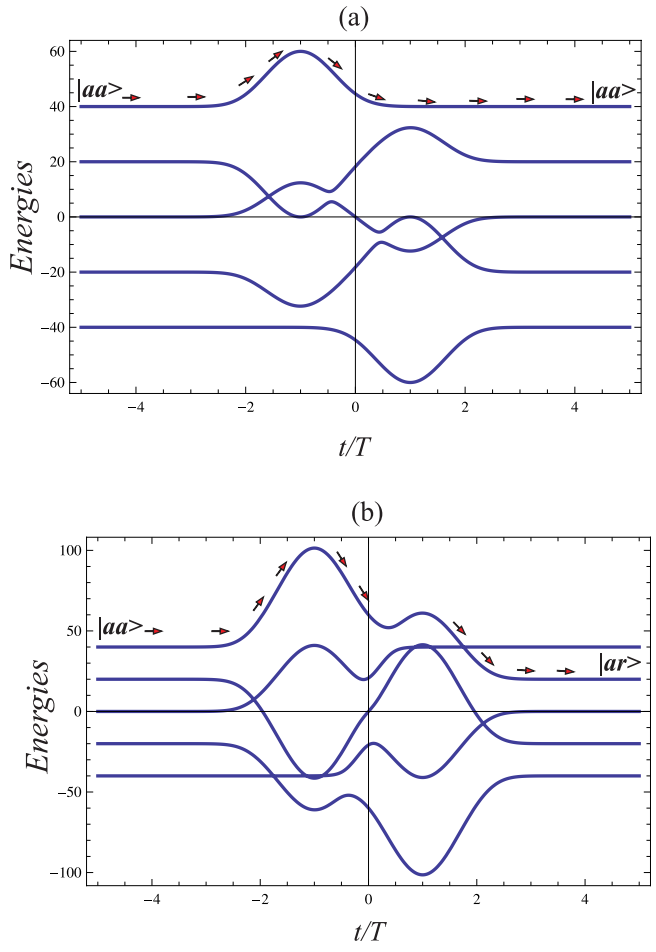

Fig. 5. Two-atom eigenstates of the Hamiltonian (15) for $\alpha = 20$ (a) and $\alpha = 60$ (b). The initial momentum $p = 10$.

In Figure 5, we have plotted the instantaneous eigenstates of the Hamiltonian (15) for two fast atoms ($p = 10$) with the peak Rabi frequency $\alpha = 20$ (Fig. 5a) and $\alpha = 60$ (Fig. 5b). The lines do not cross but have avoided crossings, some of them cannot be seen on this scale. We stress that in our case real crossings are forbidden. This follows from the fact that the Hamiltonian (10), which is unitary equivalent to (15), can be represented as a tridiagonal matrix (see Fig. 3). For such matrices, there is a theorem that states that all the eigenvalues are simple i.e., nondegenerate if none of the off diagonal elements vanish (see e.g. [17]).

The mixing angle $\theta(t)$ rotates from $\theta(-\infty) = \frac{\pi}{2}$ to $\theta(+\infty) = 0$. We define the transfer state to be the particular eigenstate of the Hamiltonian (15) and system evolves from this state. The paths (the arrows are plotted as a guide to the eye) of the transfer-state eigenvalue are shown in Figure 5. When the evolution is adiabatic the population remains in one eigenstate of the Hamiltonian (15) (see Fig. 5a). The diabatic evolution of the transfer state may occur through some sufficient weakly avoided crossings (see Fig. 5b) and is responsible for the transition $|aa\rangle \to |ar\rangle$. During such diabatic evolution, the transfer state changes from one adiabatic eigenstate to another. Hence, the key to successful population transfer $|aa\rangle \to |ar\rangle$ is a combination of the overall adiabatic evolution with some localized diabatic process. To this end we examine the time evolution of the transfer-state energy at each instant.

The changes in the state of atoms can be thought as a three step process: the atoms interact with the pulse $\Omega_P(t)$ (I-step), both pulses interact with atoms (II-step) and at the end of the interaction the pulse $\Omega_S(t)$ interacts with atoms (III-step). The "diabatic" crossings appear at first and third steps corresponding to small values of $\sin 2\theta$.

Hence, at the first and last steps, when the overlap between the Rabi frequencies is negligibly small ($\sin 2\theta \to 0$) the spectrum of the Hamiltonian can be specified by the number of dark bosons $N_D = D^\dagger D$ with eigenvalues $0, 1, \ldots, N$. After simple algebra one finds the spectrum

$$E_k^{(+)} = 2p\left(2k - N + \frac{1}{2}\right)\cos 2\theta + \sqrt{(p\cos 2\theta)^2 + \Omega_0^2 (N-k)}, \tag{15}$$

$$E_k^{(-)} = 2p\left(2k - N + \frac{1}{2}\right)\cos 2\theta - \sqrt{(p\cos 2\theta)^2 + \Omega_0^2 (N-k)}, \tag{16}$$

$$E^{(0)} = 2pN\cos 2\theta, \tag{17}$$

of the Hamiltonian

$$\widetilde{H}_{\mathrm{JC}} = 2p(2N_D - N)\cos 2\theta + 2p\sigma^\dagger\sigma^-\cos 2\theta \tag{18}$$

$$+ \Omega_0\left(B^\dagger\sigma^- + B\sigma^+\right), \tag{19}$$

where $k = 0, 1, \ldots, N-1$ is the occupation number in the dark boson mode.

Figure 6 displays the eigenvalue curves (15)–(17) in comparison with the exact energies (obtained numerically) for small ($\alpha = 20$), intermediate ($\alpha = 50$) and large ($\alpha = 160$) values of α. They are in quite good agreement for early and late times. To understand the dynamics we examine the time evolution of the transfer-state energy $E_0^{(+)}$(the dark-bosons are absent). Note that, at very early times, the transfer-state energy coincides with $2pN$ ($\cos 2\theta \to -1$ as $t \to -\infty$). Figure 6 shows a complex energy diagram with numerous real or sufficient weakly crossings between $E_k^{(\pm)}$ and $E^{(0)}$. At crossings with sufficiently large interaction $2p\left(D^\dagger B + B^\dagger D\right)\sin 2\theta$ Landau–Zener transitions between diabatic states will occur. As can be seen from Figure 6a for small α the population flows from $E_0^{(+)}$ through all intermediate energies $E_k^{(\pm)}, k = 1, 2, \ldots N-1$ and reaches at the end $E^{(0)} \to 2pN$ ($\cos 2\theta \to 1$ as $t \to +\infty$). It follows from equations (15)

and (17) that the crossing between $E_{N-1}^{(+)}$ and $E^{(0)}$ occurs at

$$\cos 2\theta\left(t_c\right) = \frac{\Omega_0\left(t_c\right)}{2\sqrt{2}p}, \tag{20}$$

and does not depend on N. Hence, if (for Gaussian pulses (9) with $\tau = T$)

$$\left[\Omega_0\left(t\right)\right]_{\max} \approx \alpha << 2\sqrt{2}p, \tag{21}$$

i.e. $\cos 2\theta\left(t_c\right) << 1$ $\left(\sin 2\theta\left(t_c\right) \approx 1\right)$ the interaction $2p\left(D^{\dagger}B + B^{\dagger}D\right)\sin 2\theta\left(t_c\right)$ connects these two states and turns this crossing into an avoided one, as shown by the blue lines in Figure 6a. Thus, when the evolution is adiabatic the population remains in one and only one adiabatic eigenstate of the Hamiltonian (10). In other words, the Doppler shift p prevents any excitation in the system. The atomic system remains in its initial state. This explains the threshold behavior of the population transfer efficiency depending on α in Figure 4. While for moderate strong-driving regime, diabatic evolution of the transfer state may occur through some suffciently weakly avoided crossings, when

$$2\sqrt{2}p \lesssim \alpha \lesssim \frac{2\sqrt{6}}{\sqrt{6-\sqrt{33}}}p \tag{22}$$

significant transfer to state with $E_{N-1}^{(+)} \to 2p\left(N-1\right)$ i.e. the state $|ar\rangle$ observed (see Fig. 6b). The right hand side of the inequality (22) defines the regions in the parameter space where a crossing between diabatic energies $E_{N-2}^{(+)}$ and $E_{N-1}^{(+)}$ is allowed, while the left side prevents a crossing of $E_{N-1}^{(+)}$ and $E^{(0)}$ at times t where the interaction $2p\left(D^{\dagger}B + B^{\dagger}D\right)\sin 2\theta\left(t\right)$ is strong. Strictly speaking, the inequalities (22) define the borders of high and low transfer efficiency to the state (2) . As α increases further $\alpha \gtrsim \frac{2\sqrt{6}}{\sqrt{6-\sqrt{33}}}p$, the transition probability to the state $\left|\underbrace{a...a}_{N-2}br\right\rangle$ with energy $E_{N-2}^{(+)} \to 2p\left(N-3\right)$ approaches unity (see Fig. 6b). In the limit of large $\alpha \gtrsim 8p\sqrt{N}$, as can be seen from equation (15) (see Fig. 6c) the transfer-state energy $E_0^{(+)}$ crosses with all $E_k^{(+)}$ diabatically. Next we note that according to (15), at the end of the interaction the transfer-state energy becomes equal to $-2p\left(N-1\right)$. As a consequence the transfer state would make the transition to state $\left|\underbrace{b...b}_{N-1}r\right\rangle$ i.e. the state (1).

From the above qualitative discussions it is clear that the required laser Rabi frequencies for successful population transfer to the state $\left|\underbrace{a...a}_{N-1}r\right\rangle$ i.e. the state (2) is the independent of system size. This prediction is verified by numerical calculations of the population of the state (2) at the end of the interaction.

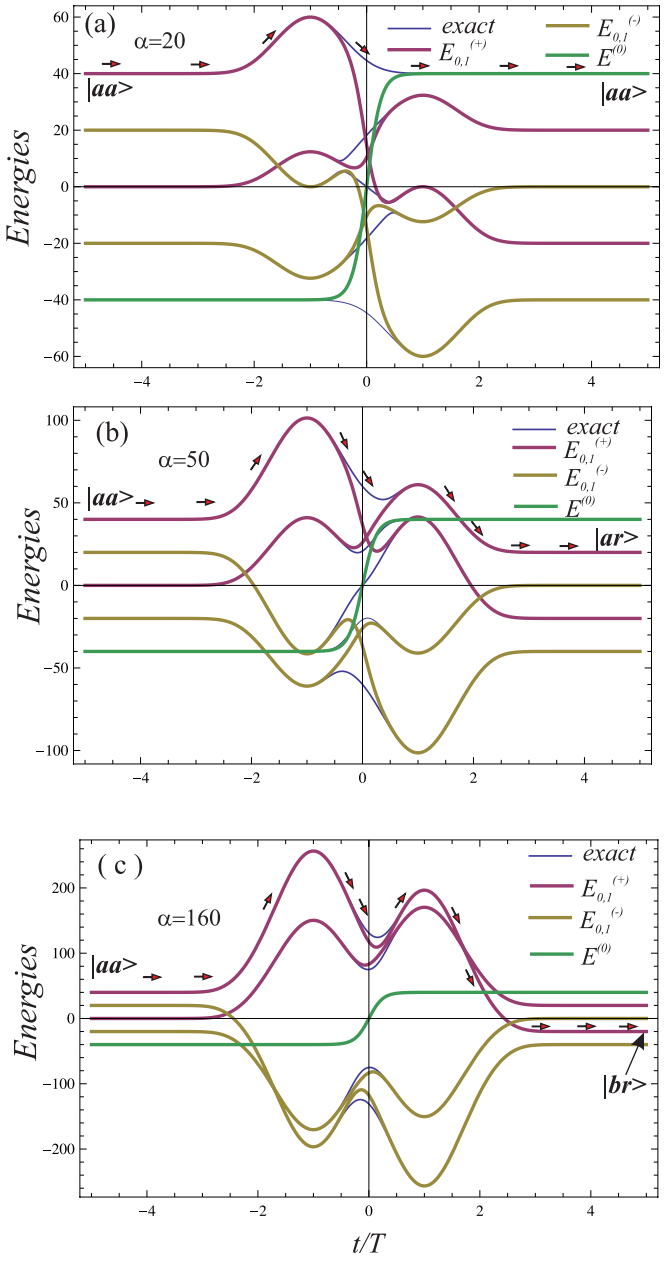

Fig. 6. Energies of Hamiltonians ($p = 10$) (15) (the blue lines) and (18) (red, yellow and green lines) for two atoms, for (a) $\alpha = 20$, (top frame), (b) $\alpha = 50$ (middle frame), (c) $\alpha = 160$ (bottom frame).

Figure 7 displays the calculated final population of $\left|\underbrace{a...a}_{N-1}r\right\rangle$ with the Jaynes–Cummings Hamiltonian (10) as a function of α for different number of atoms N. Indeed, as seen in the above figure, nearly the complete population transfer to the state (2) is observed within a certain range of α. This was predicted by the analytical estimates (22). Moreover, the width of the region of large transfer

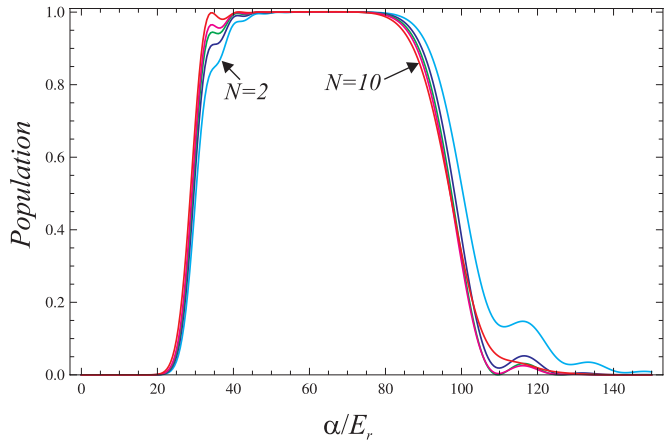

Fig. 7. Final-state population of the target state (2) for $N = 2, 3, 4, 5$ and 10 atoms as function of α. Other parameters are $\tau = T$, $p = 10$.

efficiency is not sensitive to the number of atoms. Looking at Figures 2 and 4 (two atoms), we may argue that a similar behavior is to be expected using the Hamiltonian (8) with a very large U_0. However, the numerical simulations become difficult as the number of atoms increases. We hope to return to this topic in a future publication.

6 Conclusion

In this work, an efficient and robust method to generate the entangled state (2) for a strongly interacting, moving Rydberg atomic ensemble has been proposed. It was shown that when the Doppler shift is much larger than the photon recoil energy, the entangled state (2) can be created by two laser pulses with peak amplitudes independent of system size. It was also shown that the proposed method is reminiscent of an adiabatic passage: combination of the adiabatic evolution with some localized diabatic one. Moreover, we found that the symmetric entangled atomic states can be labeled by different photon recoil momenta. This allows the detection of these states by making use of a time-of-flight analysis of atoms.

The author thanks M. Fleischhauer, K. Bergmann and B.W. Shore for helpful discussions. Financial support by the DFG through the priority program GiRyd, SPP 1929 is gratefully acknowledged.

References

1. D. Jaksch, J.I. Cirac, P. Zoller, S.L. Rolston, R. Cote, M.D. Lukin, Phys. Rev. Lett. **85**, 2208 (2000)
2. M.D. Lukin, M. Fleischhauer, R. Cote, L.M. Duan, D. Jaksch, J.I. Cirac, P. Zoller, Phys. Rev. Lett. **87**, 037901 (2001)
3. M. Saffman, T.G. Walker, K. Mølmer, Rev. Mod. Phys. **82**, 2313 (2010)
4. R. Raussendorf, D.E. Browne, H.J. Briegel, Phys. Rev. A **68**, 022312 (2003)
5. N.V. Vitanov, A.A. Rangelov, B.W. Shore, K. Bergmann, Rev. Mod. Phys. **89**, 015006 (2017)
6. N.V. Vitanov, M. Fleischhauer, B.W. Shore, K. Bergmann, Adv. At. Mol. Opt. Phys. **46**, 55 (2001)
7. B.W. Shore, Acta Phys. Slovaca **63**, 361 (2013)
8. R.G. Unanyan, M. Fleischhauer, Phys. Rev. A **66**, 032109 (2002)
9. D. Møller, L.B. Madsen, K. Mølmer, Phys. Rev. Lett. **100**, 170504 (2008)
10. T. Opatrný, K. Mølmer, Phys. Rev. A **86**, 023845 (2012)
11. T. Keating, Ch.H. Baldwin, Y.Y. Jau, J. Lee, G.W. Biedermann, I.H. Deutsch, Phys. Rev. Lett. **117**, 213601 (2016)
12. E. Jaynes, F. Cummings, Proc. IEEE **51**, 89 (1963)
13. B.W. Shore, P.L. Knight, J. Mod. Opt. **40**, 1195 (1993)
14. T.M. Weber, M. Hoening, T. Niederpruem, T. Manthey, O. Thomas, V. Guarrera, M. Fleischhauer, G. Barontini, H. Ott, Nat. Phys. **11**, 157 (2015)
15. L. Beguin, A. Vernier, R. Chicireanu, T. Lahaye, A. Browaeys, Phys. Rev. Lett. **110**, 263201 (2013)
16. M. Fleischhauer, A. Imamoglu, J. P. Marangos, Rev. Mod. Phys. **77**, 633 (2005)
17. J. Stoer, R. Bulirsch, *Introduction to Numerical Analysis* (Springer-Verlag, New York, 1980)